Optimized local synthetic conditions induce size reduction and phase purification in [Fe(Htrz)2(trz)](BF4)n spin crossover particles

Tristan Castel, Anaïs Marchetti, Felix Houard, Nathalie Daro, Mathieu Marchivie, Guillaume Chastanet, Kevin Bernot

Optimized local synthetic conditions induce size reduction and phase purification in $\{[Fe(Htrz)_2(trz)](BF_4)\}_n$ spin crossover particles

Tristan CASTEL[a], Anaïs MARCHETTI[b], Félix HOUARD[a], Nathalie DARO[b], Mathieu MARCHIVIE[b], Guillaume CHASTANET[b,], Kevin BERNOT[a,c]*.*

a) Univ. Rennes, INSA Rennes, CNRS, ISCR (Institut des Sciences Chimiques de Rennes), UMR 6226, F-35000 Rennes, FRANCE.

b) Univ. Bordeaux, CNRS, Bordeaux-INP, ICMCB, UMR 5026, F-33600 Pessac, FRANCE

c) Institut Universitaire de France, 1 rue Descartes, 75005, Paris, FRANCE

Keywords: Spin crossover nanoparticles, sonochemistry, sonocrystallization

ABSTRACT. The well-known synthesis of the two polymorphs of the $\{[Fe(Htrz)_2(trz)](BF_4)\}_n$ spin crossover coordination polymer is explored with new template-free methods that allow a control over the local synthetic conditions. A “one-pot” synthesis approach is developed, in which the solid reactants are mixed together before the addition of the solvent, which is expected to generate instantaneous supersaturation conditions favoring the nucleation of particles over their

growth. In a second method, the addition of ultrasound pulses promotes the appearance of local "hot spots" that affect the local temperature and allow exploring a different region of the concentration-temperature phase diagram, leading to an increase in the phase purity of the product. These two syntheses are compared to the classical method in which the reactants are first dissolved in separate solutions before being mixed. The use of a one pot synthesis, with or without ultrasound pulses induces a downsizing of the particles size by a factor 500 on their volume. The addition of ultrasound pulses allows moving from a mixture of polymorphs **I** and **II** of this compound to a pure phase **I**. These approaches open the way to more studies on the control over the size, or phase purity in such molecular compounds, without the use of any surfactant.

INTRODUCTION

Switchable compounds and, among them, spin crossover (SCO) molecules and materials are at the core of many research efforts focusing on molecule-based devices including molecular memories, pressure, temperature or gas sensors, optoelectronic devices and molecular actuators [1-4]. SCO coordination complexes are interesting for these types of applications due to their ability to switch between two electronic configurations (a low spin state, LS, and a high spin state, HS) by the application of an external stress (temperature, pressure, light, electric or magnetic field…), which causes significant changes in the optical, magnetic, mechanical, and dielectric properties of the material. At the molecular level, one molecule can be in either one of the two states but in the solid state, cooperative interactions may drive the occurrence of hysteretic properties resulting in a memory effect of interest for many applications [5]. The evolution of this memory effect upon reduction of the material dimensions down to nanoparticles or thin films has been the subject of

many studies in the last 20 years to evaluate the possibilities of integrating such systems into operating electronic devices [6,7]. As a general observation, the memory effect can be maintained, even if reduced in operating range, even in particles as small as a few tens of nanometers [8-11].

Several synthetic strategies were explored to reduce the particle size in a controlled way. Three main routes can be used: the template-free, the soft-template and the hard-template approaches. The template-free method is principally based on the efficient production of nuclei preventing as much as possible their growth as large particles. This can be achieved by controlling the supersaturation conditions, by either playing on the presence of non-solvent or changing the temperature. It is generally achieved in *classical syntheses* starting from separate solutions of reactants and controlling their mixing *via* magnetic stirring [12,13] but not only. Indeed, spray drying [14], flow chemistry [15] coupled to supercritical CO_2 [16] and microfluidic [17] methods have also been used in recent years. The extent to which one can control the crystallite size with these methods depends a lot on the compound under study and its bulk crystal structure. While it is has been clearly demonstrated for Prussian blue analogs [18], it is less obvious for spin crossover compounds like the ones belonging to the triazole coordination polymer family $[Fe(Rtrz)_3]X_2$ (Rtrz = 1-R-1,2,4-triazole). This latter family, however, is probably one of the most studied family of SCO compounds as it affords room temperature switching properties. To solve the issues encountered with template-free methods, many studies have therefore been undertaken to obtain nanoparticles (NPs) of adjustable sizes and morphologies using templates. For instance, hard-templates studies allows obtaining NPs of around 2-5 nm of the one-dimensional (1D) $[Fe(Htrz)_2(trz)](BF_4)$ within the pores of silica xerogels [19] or preformed silica monoliths [20]. Similarly, a large number of studies considered the soft-template approach, using various surfactants or polymers in which nanometric pools constrain the growth of the particles. These

pools can be stabilized in apolar solvents through reverse-micelle synthesis using either charged or neutral surfactants. For example, regarding the specific case of the $[Fe(Htrz)_2(trz)](BF_4)$ compound, this strategy provided in a controlled way, particles ranging from 6 nm when using the charged surfactant NaAOT (sodium dioctyl sulfosuccinate) [8,21] to hundreds of micrometers using neutral Tergitol [22]. Beside this micellar approach, the use of organic polymers has also been successful in obtaining small NPs of controlled size for various spin crossover compounds. For instance, block copolymers (BCPs) can form micellar structures because of the strong difference in solubility between one block and the other in a given solvent. Depending on the ratio between each block, the size and amount of NPs embedded in this polymer can be tuned [23,24]. Additionally, other organic polymers have been used such as PVP (polyvinylpyrrolidone), PVA (PolyVinyl Alcohol), PEG (PolyEthylyneGlycol), triton… with a less efficient control over the particle size [25,26]. The recent review by Salmon and Catala reports in a more exhaustive way the various approaches and uses of such SCO NPs [27].

One important aspect of the use of templates, besides the good control over the size, morphology and even polymorphism, lies in the difficulty to get rid of this template afterwards. This is even not possible for some hard templates or charged surfactants. *In fine*, it may alter both the composition and the properties of the obtained compound.

As part of our recent work on template-free approaches, in this paper, we explore and compare two alternative methods to obtain $[Fe(Htrz)_2(trz)](BF_4)$ particles of reduced size: the *one-pot synthesis* coupled or not with *sonocrystallization*. Their influence over the size, morphology, phase purity and magnetic switching properties are discussed and compared with *classical syntheses*.

EXPERIMENTAL SECTION

Synthesis

Chemicals were used as purchased, without further purification. Three types of syntheses were performed: a *classical synthesis* in solution (**a**) a *one-pot synthesis* (**b**) and finally, a *one-pot synthesis* coupled with an *ultrasonic synthesis* (**c**). These three reactions were performed for concentrations of 0.5 mol/l and 0.75 mol/l of $Fe(BF_4)_2$. The concentration of 1,2,4-1*H*-triazole was calculated to be in slight excess (10 %) compared to the stoichiometric conditions. The samples were named **1a**, **1b** and **1c** for 0.5 mol/l of $Fe(BF_4)_2$ and **2a**, **2b** and **2c** for 0.75 mol/l.

Classical syntheses ("classical" **a**) were adapted from ref. 28 and performed by adding in one step an aqueous solution of 1,2,4-1*H*-triazole (10 mL) into an aqueous solution of well dissolved $Fe(BF_4)_2$ (10 mL) with 10 mg of ascorbic acid in a 50 ml beaker. The mixture was stirred (magnetic stirring) during 10 min at 60 °C.

One-pot syntheses ("one pot" **b**) were implemented by putting the reactants powders in stoichiometric proportions (same quantity as the *classical synthesis*) in the same beaker, then adding 20 ml of water at 60 °C. The resulting mixtures were let 10 min under stirring (magnetic stirring) at this temperature.

Ultrasonic syntheses ("one pot US" **c**) were realized putting the reactants powders in the same beaker and then adding 20 ml of water at 60 °C. The resulting mixtures were immediately submitted to sonication for 10 min at 60 °C. The ultrasonication was performed using a Hielscher UP400 St sonicator that operates at 24 kHz. The S24d3 sonotrode was placed in the beaker at a fixed position and the temperature monitored with a thermal sensor immersed at ≈ 0.5 cm of the sonotrode. In order to stabilize the temperature plateau at 60 °C (± 1 °C) a 90 % sonication pulse (0.9 s sonication, 0.1 s of silence) was used. Each pulse delivers 24 J to the solution (total amount

of 14.40 kJ for 10 min crystallization). It has to be noted that, contrary to syntheses **a** and **b** for which the temperature is stabilized by using an external heating source, the temperature in synthesis **c** is stabilized by the internal sonication pulses, without any external contribution.

All the solutions were filtered (por. 5) after synthesis. The powders were then washed with ethanol and filtered again three times. The powders were then dried at room temperature under ambient atmosphere.

Powder X-ray diffraction (PXRD)

PXRD samples were prepared on silicon sample holders. The measurements were performed on a PANalytical X'pert PRO MPD diffractometer with a Bragg-Brentano θ-2θ geometry equipped with a Ge (111) front monochromator, and a perfectly monochromatic Cu $K\alpha_1$ (λ = 1.54059 Å) radiation. The detector was a multi-channel detector X'Celerator, the working voltage 45 kV and the working current 40 mA. Refinements of the powder patterns were performed using the so called profile matching refinement using the Lebail method [29]. All patterns were refined using the polymorph **I** cell parameters as starting point. Polymorph **II** cell parameters were introduced for the powders prepared with the "*one pot*" (b) method to improve the refinement results.

The refined variables were: the unit cell parameters, sample displacement, and peak broadening due to coherent domain size and micro-strain effects. According to the lack of data at high resolution (especially for nanosized powders) the micro-strain parameter was fixed to the one that was obtained for well-crystallised samples (*classical synthesis*, micro-strain = 0.25 %). The peak broadening then accounts only for size effects. As polymorph **II** was found in very small quantities when present, size broadening was refined anisotropically only for polymorph **I** leading to an estimation of coherent domain size along a, b and c directions for **I** and only a mean isotropic value for **II**.

Transmission Electron Microscopy (TEM)

Transmission Electronic Microscopy (TEM) images were acquired on a JEOL JEM 1400 Plus microscope at 60 kV (LaB6source) with a Gatan Smart Orius 1000 camera at the PLACAMAT platform (UAR 3626).

Scanning Electron Microscopy (SEM)

SEM analysis was performed with a JEOL JSM 7100 F at 10 kV (CMEBA from ScanMAT, Rennes).

Dynamic Light Scattering (DLS)

Dilute solutions (C_m = 0.1 mg/ml) were prepared by dispersing the particles in ethanol with a 1 min sonication step. The dispersed solutions were then filtered on sintered silica filters (por. 4) to avoid the presence of large dust particles. DLS measurements were performed on a VASCO KIN™ particle size analyzer (Cordouan Technologies, Pessac, France), with a 635 nm laser diode (50 mW) at a scattering angle of 170°. The sample positions were fixed manually with respect to the laser head, in order to minimize the signal-to-noise ratio *i.e.* maximize the β parameter. Acquisitions and analyses of the correlograms (Figures SI2-5) were based on the continuous multimodal Sparse Bayesian Learning (SBL) algorithm (in number) provided by the Nano Kin™ software.

Magnetic measurements

Magnetic susceptibility measurements were performed on a EZ7 MicroSense Vibrating Sample Magnetometer (VSM). The powders were put in a tin capsule (Ø 3.5 mm), and affixed to the tip of a quartz rod (Ø 3 mm) with Teflon tape. Each sample was submitted to 4 thermal cycles between 300 K and 420 K at 5 K/min under a magnetic field of 18000 Oe and a 0.34 m^3/h N_2 flow.

RESULTS AND DISCUSSION

Polymorphism in $[Fe(Htrz)_2(trz)](BF_4)$

The compound of interest in this study is the one-dimensional coordination polymer $[Fe(Htrz)_2(trz)](BF_4)$. It has been widely studied since its discovery in 1977 [30] mainly because it exhibits a well-defined and large hysteresis cycle above room temperature, which is of interest for memory storage. Two forms of this compound were initially reported on the basis of their magnetic properties [28]. The first one (**I**) shows a large hysteresis of *ca*. 40 K centered at 370 K and the second one (**II**) presents a narrower hysteresis of *ca*. 15 K, centered at 330 K. The crystal structure of these polymorphs has recently been elucidated from powder X-ray diffraction (PXRD) showing a one-dimensional arrangement of $[Fe(Htrz)_2(trz)]^+$ chains separated by BF_4^- anions [12,31]. Both polymorphs crystallize in the Pnma space group at room temperature (in the LS state) with a = 17.294(6) Å, b = 7.337(2) Å, c = 9.182(3) Å and V = 1165.1(6) $Å^3$ for **I** and a = 16.691(4) Å, b = 7.338(1) Å, c = 9.482(3) Å and V = 1161.3(5) $Å^3$ for **II**, in the LS state. From an experimental point of view, polymorphs **I** and **II** can be discriminated quite easily using their powder X-ray diffractograms. A single peak is seen around 10.6 ° in 2θ on Cu-Kα diffractograms for **II** as a signature of the very close 200 and 101 hkl reflections while for **I** these peaks are clearly resolved due to the modification of a and c parameters (see figure 2d). From the crystallographic point of view, the difference between these two forms may come from the presence of a disorder in the position of the deprotonated triazole ligand. This might be at the origin of the less defined morphologies of the particles of **II** compared to the rod shape of **I**. In any case, this clear picture, can be blurred at the nanoscale by a broadening of the peaks, leading to a merging of the double peak in **II** into a wide shouldered single peak. Differences also appear around 19.2°, 24° and 25°

with several peaks for **I** and less and broader peaks for **II**. Therefore, profile matching (at least) or Rietveld refinement of the diffractograms is highly recommended to clearly identify both polymorphs as soon as their powders are nanocrystalline.

From the synthetic point of view, both polymorphs can be synthesized in different conditions either by changing the solvent [28] or the concentration and temperature [12]. As a general trend, the higher the temperature and the lower the concentration of reactants, the more the polymorph **I** is favored [12], for a given solvent mixture (Figure 3). All these syntheses start from the dissolution of the reactants, especially the iron salt dissolved in water (or in a water/ethanol mixture). This dissolution tends to form the hexa aqua iron complex and to generate the coordination polymer, a ligand exchange must occur: the triazole displaces the water molecules. Depending on the concentration and temperature, this ligand exchange step may slow down the reaction, favoring the growth of particles more than their nucleation and providing powders with quite big crystallites.

Comparison of the synthetic strategies.

In this paper, we target a size reduction of the $[Fe(Htrz)_2(trz)](BF_4)$ particles using as reference the *classical* synthesis (synthesis **a**). We used two different concentrations of reactants: (0.5 mol/l or 0.75 mol/l of $Fe(BF_4)_2$ at T = 60 °C to be able to extract sound conclusions. According to the Temperature-Concentration phase diagram obtained for this compound (Figure 3) [12], in these conditions, the pure phase **I** of $[Fe(Htrz)_2(trz)](BF_4)$ is expected.

To decrease the particles size, the preparation method was modified to impact either particles nucleation or growth during the synthesis process. On one hand, the effect on nucleation was tested using a *one-pot synthesis* (synthesis **b**) that is known to favor the formation of nuclei by providing rapid supersaturation conditions. The objective is to prevent the formation of hexa aqua complexes

that slows down the water-ligand exchange and therefore the formation of the nuclei. It consists in mixing the reactants' powders together, adding the solvent, and applying a magnetic stirring at 60 °C. On the other hand, the effect on particle growth is tested by adding *sonocrystallization* (synthesis **c**) [32] to the *one-pot synthesis*. We replaced magnetic stirring by pulsed ultrasonic waves whose power and emission rates are tuned to stabilize a temperature plateau at 60 °C (see experimental section). This technique is known to reduce the induction time, *i.e.* the time elapsed between superstaturation and the growth of the first crystals [33]. Consequently, it avoids both secondary crystallization (by destroying less robust crystals germs) and high particle size (by providing homogeneous germ dimensions and fragmenting particles with too low aspect ratio).

The data collected in terms of particles' sizes, coherent domain sizes, phase and switching temperatures for samples **1a**, **1b** and **1c** (0.5 mol/l of $Fe(BF_4)_2$) and **2a**, **2b** and **2c** (0.75 mol/l of $Fe(BF_4)_2$) are reported in Table 1.

Influence of the synthetic conditions on particle dimension and morphology

Table 1. Summary of the particles characteristics and properties for $Fe(BF_4)_2$ concentration of 0.5 mol/l (**1**) and 0.75 mol/l (**2**)

			Cristallographic coherent domains size[(a)]		*Particles size[(b)]*		*V of the particles* 10^6 *nm*^{3} *[(c)]*	*Switching temperatures[(d)]*		
name	Synthesis	Phase	along b (nm)	along a and c (nm)	TEM L × l (nm x nm)	DLS (nm)		$T_{1/2}$ ↑ (K)	$T_{1/2}$ ↓ (K)	ΔT (K)
1a	Classical	**I**	265	100	2830 x 200	-*	113	387	356	31
1b	One pot	**I**	63	30-40	107 × 43	108	0.20	382	352	30
		II		30						
1c	One pot US	**I**	60	20-30	142 × 42	130	0.25	382	353	29
2a	Classical	**I**	220	90-110	1471 × 182	-*	48	394	355	39
2b	One-pot	**I**	50	30	97 × 42	152	0.17	382	347	35
		II		30						
2c	One-pot US	**I**	60	30	138 × 42	225	0.24	387	349	38

*(a) Obtained from the profile matching of the powder X-ray diffractograms; (b) Obtained either from DLS or analysis of TEM images on more than 50 particles; (c) Estimated from the volume of a rectangular parallelepiped L×l²; (d) Measured using a vibrating sample magnetometer. * Due to the strong anisotropy of the particles, the obtained values are not reliable (see SI).*

Concerning the *classical* synthesis, under these reaction conditions, rod-shaped 2.8 µm (**1a**) and 1.5 µm (**2a**) long particles are obtained, with a large size distribution (Figures 1, SI1). The values obtained by DLS are less relevant in the present case because of the highly anisotropic shape of the particles (aspect ratio above 10) while the DLS data result from the use of spherical models. In contrast, the *one-pot syntheses* (both with and without ultrasounds), yield particles of around 100 nm in length (Figures 1, SI1), as evidenced by SEM, TEM and DLS analyses. There is clearly a drastic effect of changing the synthetic methodology on the particle size. Indeed, the length and volume (assuming rectangular parallelepiped shapes) of the particles is reduced by a factor 25 and 500, respectively, for conditions **1**, and by a factor of 12 and 250, respectively, for conditions **2**. The addition of ultrasound pulses during the synthesis has little effect on the particle size, and only has a significant effect on the length (and not the width) of the particles, which results in an increase in the aspect ratio from ~ 2.5 to ~ 3.5. Moreover, it increases the width of the particle size distribution. Indeed, the standard distribution σ (using a normal law), increases from ~ 20 nm (syntheses **b**) to ~ 40 nm (syntheses **c**).

This clearly shows that in these operating conditions, and contrary to what was previously observed on similar 1D coordination compounds [34], the sonication does not operate in a sonocrystallization regime that is known to reduce particle size distribution. Sonofragmentation (breakage of large crystallite) [35] may occur here. Moreover, applying ultrasounds provides local heat. Indeed, while a temperature plateau of T = 60 °C is measured during the synthesis, the collapse of cavitation bubbles created by the compression and expansion of the acoustic waves induces “hot spots” in the solution with very high local temperatures and pressures (T ≈ 5000 K, P ≈ 1000 atm) [36-38]. This local heat might be in favor of the observed increase in particle size as already reported for this compound [22].

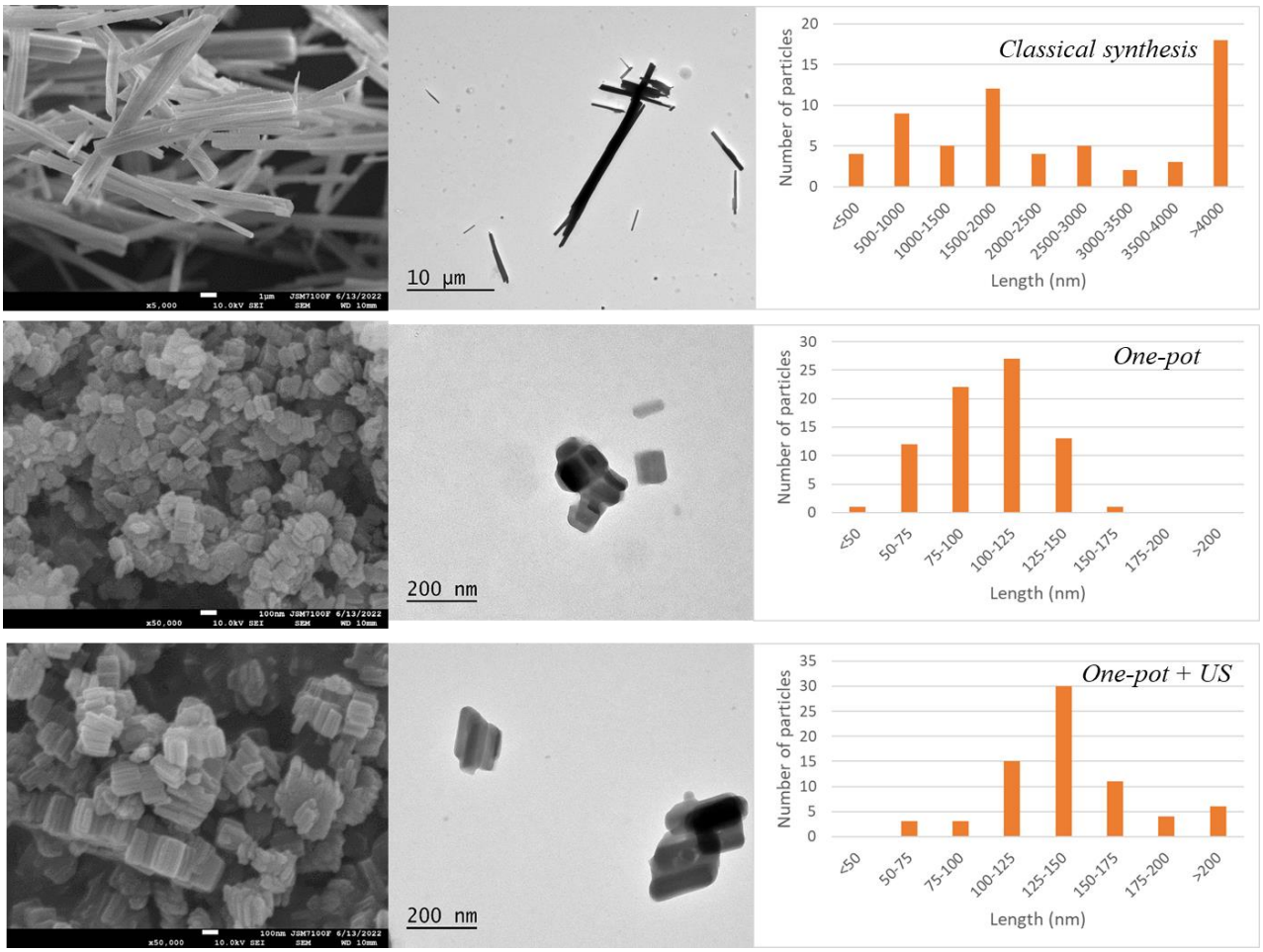

Figure 1. SEM (left, x 5k or 50k) and TEM (right) images of samples **1a** (top), **1b** (center), **1c** (bottom) with their respective length size distributions obtained from TEM analyses over more than 60 particles (inset).

Influence of the synthetic conditions on polymorphism and phase purity

Powder X-ray diffraction patterns were recorded for each compound (Figures 2, SI6). While the clear typical features of phase **I** are observed for the samples obtained using the *classical synthesis*, it is less obvious for the other diffractograms. This could be due to a size reduction effect (in agreement with the SEM and TEM pictures in Figure 1) and/or a mixture of phases. The refinement of the diffractograms is then necessary to clarify the situation. For the sample issued from the *classical synthesis*, the pure polymorph **I** is obtained, with crystallographically coherent domains above 200 nm along the b axis, which corresponds to the direction of the 1D $[Fe(Htrz)_2(trz)]^+$ chains (Figures 2, SI6). Concerning the *one-pot syntheses*, the diffractograms can be refined using the polymorph **I** parameters, but are significantly improved by the introduction of a fraction of polymorph **II**. These particles correspond then mainly to polymorph **I** with a small amount of polymorph **II**. The coherent domain sizes refine to 63 nm (**1b**) and 50 nm (**2b**) along the b axis for polymorph **I**. With the application of ultrasounds, only phase **I** is observed while the coherent domain size along b remains unchanged at 60 nm in both **1c** and **2c** (Figures 2, SI6). Therefore, the differences between the various diffractograms are not only due to the size reduction of the particles and the coherent domain sizes as one can conclude at first glance, but also to a phase purity issue. This is clearly a point of vigilance while looking at diffractograms in general, and in the case of the present compound in particular, when polymorphism is present.

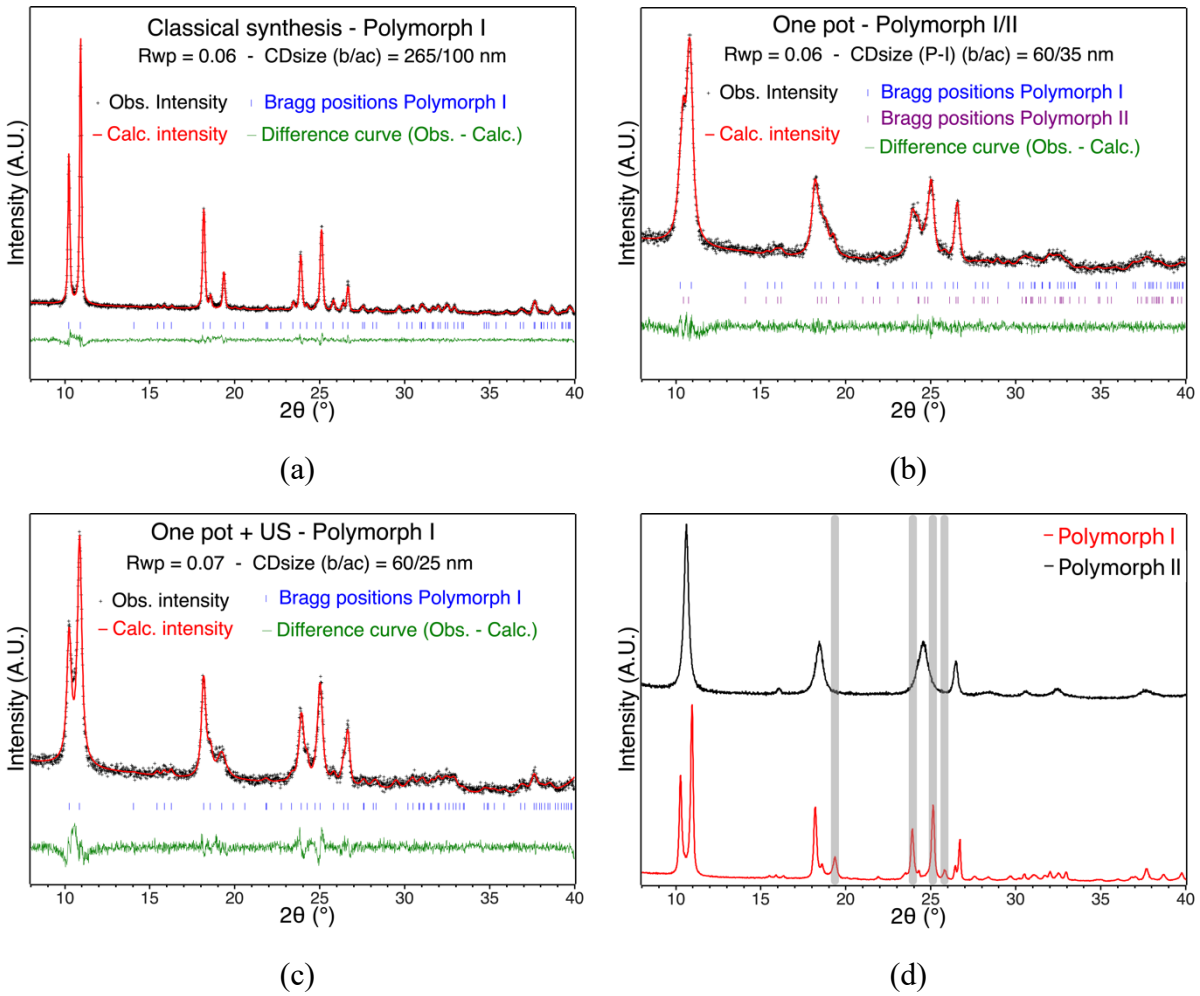

Figure 2. PXRD pattern for samples (a) **1a,** (b) **1b,** (c) **1c** with profile matching refinement (Le Bail) and theoretical peak positions of phases **I** and **II**. Peak broadening can be unambiguously assigned to a size reduction and a phase impurity ("one-pot") or a size reduction only ("one-pot + US") on the basis of the refinement. Figure (d) shows the PXRD diagrams of pure polymorphs **I** and **II** showing some specific peaks of polymorph **I** (grey bands).

These changes in the nature of the phases obtained with different reaction conditions can be explained using the known Temperature-Concentration phase diagram of this compound (Figure 3)[12]. In our concentration conditions (0.5 mol/l or 0.75 mol/l at 60 °C) the *classical synthesis*

should afford pure phase **I** (point **a**). However, both *one-pot* and *ultrasounds assisted syntheses* provide out-of equilibrium phases because local conditions are different from global one. Indeed, the *one-pot synthesis* that avoids the formation of the iron hexa aqua complex offers local high concentration conditions that drive the system toward the region where phases **I** and **II** are mixed (point **b**). Similarly, from this point, applying ultrasounds provides local heat ("hot spots" T ~ 5000 K, P ~ 1000 atm) [36-38] that allows to enter the region where only phase **I** is obtained (point **c**).

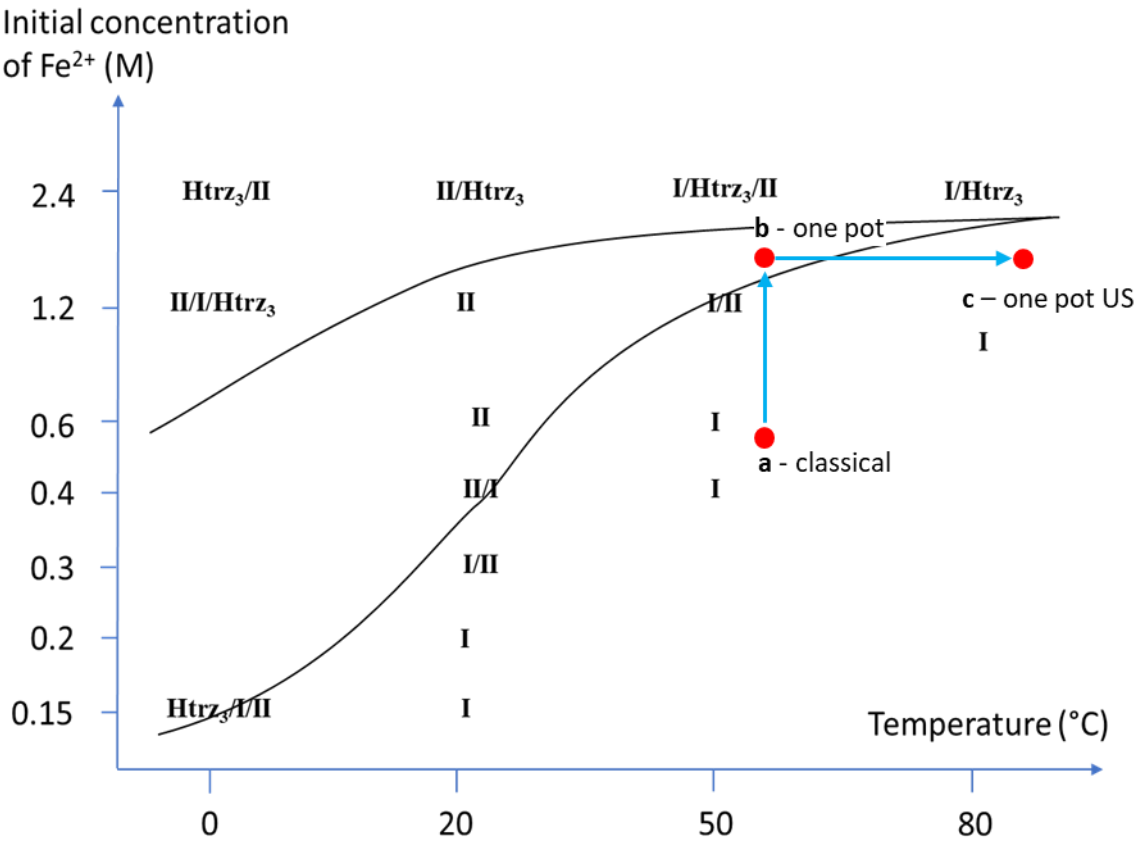

Figure 3: Concentration/temperature phase diagram of $[Fe(Htrz)_2(trz)](BF_4)$ (adapted from ref [12]) as a function of the synthetic conditions established in *classical synthetic* conditions (in the

present diagram a 60:40 water:ethanol mixture was used) with the hypothetic positions of the reaction conditions **a-c**. $Htrz_3$ indicates $[Fe(Htrz)_3](BF_4)_2$, the byproduct of the synthesis [12].

Influence of the synthetic conditions on magnetic behavior

Finally, the switching behavior of each compound was recorded using magnetometry. Figure 4 reports the thermal evolution of the product of the molar magnetic susceptibility χ_M times the temperature for **1a**, **1b** and **1c** (see figure SI7 for **2a**, **2b** and **2c**). Since this compound is known to present a first run-in cycle [28], meaning that the first warming curve is always higher in temperature than the other subsequent curves, this figure reports the fourth and stabilized cycle. With the exception of **1a** (and **2a**), the $\chi_M T$ values at 400 K are coherent with Fe(II) ions in the HS state (S = 2). At 300 K, this value decreases to around 0.75 cm^3K/mol, witnessing the presence of some paramagnetic residue, which is not surprising in the case of nanoparticles (**1b** and **1c**) where surface effects and defaults are expected to be present and influent. This temperature dependent changes in the $\chi_M T$ values indicates clearly the occurrence of spin crossover and the thermal cycling evidences thermal hysteresis for the three compounds. The reason why **1a** and **2a** exhibit lower $\chi_M T$ values than expected at 400 K is not clear and might come from the large size distribution of the particles and strongly anisotropic morphologies. The switching temperatures reported in Table 1 are different for **1a** ($T_{1/2}\downarrow$ = 356 K and $T_{1/2}\uparrow$ = 387 K) **1b** $T_{1/2}\downarrow$ = 352 K and $T_{1/2}\uparrow$ = 382 K) and **1c** ($T_{1/2}\downarrow$ = 352 K and $T_{1/2}\uparrow$ = 383 K) while the hysteresis width remains the same around 30 K. This indicates a shifting of the switching behavior towards lower temperature upon size reduction, as already reported [22]. The same behavior is observed for compounds **2a-c** (Table 1 and Figure SI7) with a slightly bigger hysteresis width. As already observed [12], despite the presence of a mixture of phases in **1b** and **2b**, no clear indication of such a mixture is observed

on the magnetic curves in agreement with the presence of only a small amount of polymorph **II** in this phases.

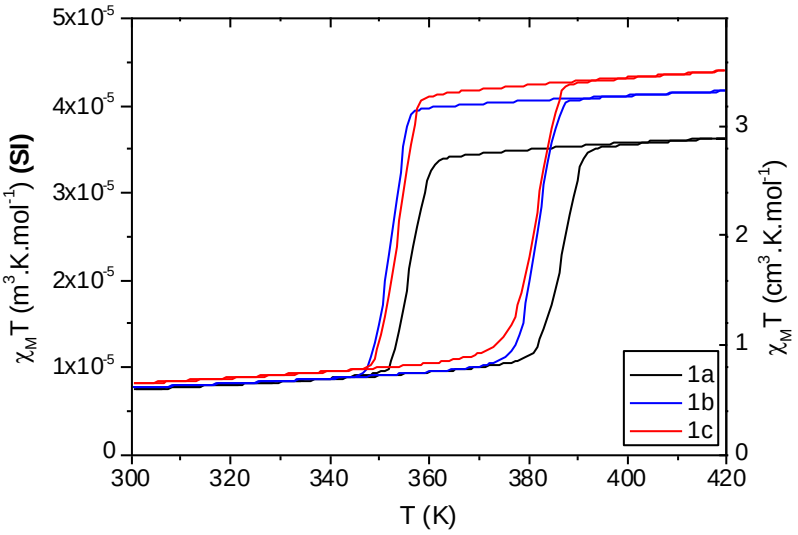

Figure 4. Thermal evolution of the product of the molar magnetic susceptibility χ_M times the temperature for **1a** (black curve), **1b** (blue curve) and **1c** (red curve). These curves correspond to the 4th cycle.

Regarding the switching properties, they are only weakly affected by the synthetic conditions, since the hysteresis width remains almost the same for methods **a**, **b** and **c**, even if a lowering of the switching temperatures is observed upon size reduction, as already reported elsewhere [22].

CONCLUSION

Among the various methods explored to reduce the size of particles, the use of simple methods sometimes provides very interesting results.

In this work we tested the influence of local changes in the synthesis conditions (concentration and temperature) on the nucleation-growth process of $[Fe(Htrz)_2(trz)](BF_4)$ SCO compounds. We

show that a *one-pot synthesis* method, that is expected to induce an increase in the local supersaturation conditions, provides a downsizing of the particles volume by a factor of 500 but results in a polymorphic sample. This polymorphism can be suppressed by adding *sonocrystallization* to the *one-pot* procedure, which has only a moderate impact on the crystallite size, but enhances drastically the phase purity. This can be explained by the increase in the local temperature induced by the sonication. Additionally, such an increase in the local temperature induces an enhanced micromixing of the reactants [39] and can be rationalized using the Temperature-Concentration phase diagram of $[Fe(Htrz)_2(trz)](BF_4)$. The study of the magnetic properties of the samples shows the expected SCO behavior for such reduced-size particles and demonstrates that efficient size reduction can be obtained with faster and greener low-energy synthetic and crystallization techniques in water.

Supporting Information. Additional TEM and SEM pictures, PXRD data and magnetic measurements can be found in the supporting information file.

AUTHOR INFORMATION

Corresponding Author

* Guillaume.chastanet@icmcb.cnrs.fr; Kevin.Bernot@insa-rennes.fr

Author Contributions

The manuscript was written through contributions of all authors. All authors have given approval to the final version of the manuscript.

Funding Sources

The French National Research Agency (ANR) project Flowswitch 2019-CE07-0022-01

ACKNOWLEDGMENT

This work was supported by the University of Bordeaux, the CNRS, the ANR FlowSwitch (2019-CE07-0022-01), and by the Region Nouvelle Aquitaine. The UAR PLACAMAT 3626 and Marion Gayot are acknowledged for the TEM. Cordouan Technologies is acknowledged for discussions on DLS measurements and L. Joanny for the SEM measurements (CMEBA, from UMS SCAN-MAT Rennes). K.B. acknowledges the Region Bretagne (Boost'ERC RECoord No. 1122), the Institut Universitaire de France (IUF) and the INSA Rennes PPI program.

REFERENCES

[1] Senthil Kumar, K.; Ruben, M.; Sublimable spin crossover complexes: from spin-state switching to molecular devices. *Angew. Chem. Int. Ed. Engl*. **2020**, *59*, 2-22.

[2] Bellec, A.; Lagoute, J.; Repain, V. ; Molecular electronics : scanning tunneling microscopy and single-molecule devices. *C.R. Chimie*, **2018**, *21*, 1287-1299.

[3] Molnar, G.; Rat, S.; Salmon, L.; Nicolazzi, W.; Bousseksou, A.; Spin crossover nanomaterials: from fundamental concepts to devices. *Adv. Mater*. **2018**, *30*, 17003862(23).

[4] Coronado, E.; Molecular magnetism: from chemical design to control in molecules, materials and devices. *Nature Rev. Mater.* **2020**, *5*, 87-104.

[5] Spiering, H.; Elastic interaction in spin crossover compounds, *Top. Curr. Chem*. **2004**, *235*, 171-195.

[6] Dayen, J.-F.; Konstantinov, N.; Palluel, M. ; Daro, N. ; Kundys, B. ; Soliman, M. ; Chastanet, G. ; Doudin, B. ; Room temperature optoelectronic devices operating with spin crossover nanoparticles. *Mater. Horiz*. **2021**, *8*, 2310-2315.

[7] Gavara-Edo, M.; Cordoba, R.; Valverde-Munoz, F. J.; Herrero-Martin, J.; Real, J. A.; Coronado, E.; Electrical sensing of the thermal and light-induced spin transition in robust contactless spin crossover/graphene hybrid devices. *Adv. Mater*. **2022**, *34*, 2202551(11).

[8] Coronado, E.; Galan-Mascaros, J. R.; Monrabal-Capilla, M.; Garcia-Martinez, J.; Pardo-Ibanez, P. ; Bistable spin crossover nanoparticles showing magnetic thermal hysteresis near room temperature. *Adv. Mater*. **2007**, *19*, 1359-1361.

[9] Raza, Y.; Volatron, F.; Moldovan, S.; Ersen, O.; Huc, V.; Martini, C.; Brisset, F. ; Gloter, A. ; Stephan, O. ; Bousseksou, A.; Catala, L.; Mallah, T.; Matrix-dependent cooperativity in spin crossover Fe(pyrazine)Pt(CN)$_4$ nanoparticles. *Chem. Comun*. **2011**, *47*, 11501-11053.

[10] Bousseksou, A.; Molnar, G.; Salmon, L.; Nicolazzi, W. ; Molecular spin crossover phenomenon : recent achievements and prospects. *Chem. Soc. Rev*. **2011**, *40*, 3313-3335.

[11] Shepherd, H. J.; Molnar, G.; Nicolazzi, W.; Salmon, L.; Bousseksou, A.; Spin crossover at the nanometer scale. *Eur. J. Inorg. Chem*. **2013**, *5-9*, 653-661.

[12] Palluel, M.; El Khoury, L.; Daro, N.; Buffière, S.; Josse, M.; Marchivie, M. ; Chastanet, G. ; Rational direct synthesis of [Fe(Htrz)$_2$(trz)](BF$_4$) polymorphs: temperature and concentration effects. *Inorg. Chem. Front*. **2021**, *8*, 3697-3706.

[13] Catala, L.; Brinzei, D.; Prado, Y.; Gloter, A.; Stephan, O.; Rogez, G.; Mallah, T.; Core–Multishell Magnetic Coordination Nanoparticles: Toward Multifunctionality on the Nanoscale. *Angew. Chem. Int. Ed*. **2009**, *48*, 183-187

[14] Daro, N.; Moulet, L.; Penin, N.; Paradis, N.; Letard, J.-F.; Lebraud, E.; Buffiere, S.; Chastanet, G.; Guionneau, P.; Spray-Drying to get spin crossover materials. *Materials* **2017**, *10*, 60(13).

[15] Robertson, K.; Flandrin, P. B.; Shepherd, H. J.; Wilson, C. C.; $[Fe(Htrz)_2(trz)](BF_4)$ nanoparticle production in a milli-scale segmented flow crystallizer *Chim. Oggi - Chem. Today* **2017**, *35*, 19-20.

[16] Daro, N.; Vaudel, T.; Afindouli, L.; Marre, S.; Aymonier C.; Chastanet, G.; One-step synthesis of spin crossover nanoparticles using flow chemistry and supercritical CO_2, *Chem. – A Eur. J.*, **2020**, 16286-16290

[17] Gonzalez-Estefan, J. H.; Gonidec, M.; Daro, N.; Marchivie, M. ; Chastanet, G. ; Extreme downsizing in the surfactant-free synthesis of spin crossover nanoparticles in a microfluidic flow-focusing junction. *Chem. Commun*. **2018**, *54*, 8040-8043.

[18] Catala, L.; Mallah, T.; Nanoparticles of Prussian blue analogs and related coordination polymers: from information storage to biomedical applications. *Coord. Chem. Rev*. **2017**, *346*, 32-61.

[19] Faulmann, C.; Chahine, J.; Malfant, I.; de Caro, D.; Cormary, B.; Valade, L.; A facile route for the preparation of nanoparticles of the spin-crossover complex $[Fe(Htrz)_2(trz)](BF_4)$ in xerogel transparent composite films. *Dalton Trans*. **2011**, *40*, 2480-2485.

[20] Durand, P.; Pillet, S.; Bendeif, E.-E.; Carteret, C.; Bouazaoui, M.; El Hamzaoui, H.; Capoen, B.; Salmon, L.; Hebert, S.; Ghanbaja, J.; Aranda, L.; Schaniel, D.; Room temperature bistability with wide thermal hysteresis in a spin crossover silica nanocomposite. *J. Mater. Chem. C.* 2013, *1*, 1933-1942.

[21] Galan-Mascaros, J. R.; Coronado, E.; Forment-Aliaga, A.; Monrabal-Capilla, M.; Pinilla-Cienfuegos, E.; Ceolin, M.; Tuning Size and Thermal Hysteresis in Bistable Spin Crossover Nanoparticles. *Inorg. Chem.* **2010**, *49*, 5706-5714

[22] Moulet, L.; Daro, N.; Etrillard, C.; Letard, J.-F.; Grosjean, A.; Guionneau, P.; Rational Control of Spin-Crossover Particle Sizes: From Nano- to Micro-Rods of $[Fe(Htrz)_2(trz)](BF_4)$. *Magnetochemistry* **2016**, *2*, 10(9).

[23] Klimm, O.; Göbel, C.; Rosenfeldt, S.; Puchtler, F.; Miyajima, N.; Marquardt, K.; Drechsler, M.; Breu, J.; Forster, S.; Weber, B.; Synthesis of $[Fe(L)(bipy)]_n$ spin crossover nanoparticles using blockcopolymer micelles. *Nanoscale* **2016**, *8*, 19058-19065.

[24] Göbel, C.; Marquardt, K.; Baabe, D.; Dreschsler, M.; Loch, P.; Breu, J.; Greiner, A. ; Schmalz, H. ; Weber, B. ; Realizing shape and size control for the synthesis of coordination polymer nanoparticles templated by diblock copolymer micelles. *Nanoscale*, **2022**, *14*, 3131-3147.

[25] Martinez, V.; Boldog, I.; Gaspar, A.B.; Ksenofontov, V.; Bhattacharjee, A.; Gutlich, P.; Real, J. A.; Spin Crossover Phenomenon in Nanocrystals and Nanoparticles of $[Fe(3\text{-}Fpy)_2M(CN)_4]$ (M^{II} = Ni, Pd, Pt) Two-Dimensional Coordination Polymers. *Chem. Mater*. **2010**, *22*, 4271-4281.

[26] Gural'skiy, I. A.; Quintero, C. M.; Molnar, G.; Fritsky, I. O.; Salmon, L.; Bousseksou, A.; Synthesis of Spin-Crossover Nano- and Micro-objects in Homogeneous Media. *Chem. Eur J.* **2012**, *18*, 9946-9954.

[27] Salmon, L.; Catala, L.; Spin crossover nanoparticles and nanocomposites materials. *C. R. Chim.*, **2018**, *21*, 1–40.

[28] Kröber, J.; Audière, J.-P.; Claude, R.; Codjovi, E.; Kahn, O.; Haasnoot, J. G.; Grolière, F.; Jay, C.; Bousseksou, A.; Linarès, J.; Varret, F.; Gonthier-Vassal, A.; Spin transition and thermal hystereses in the molecular-based materials $[Fe(Htrz)_2trz](BF_4)$ and $[Fe(Htrz)_3](BF_4)_2.H_2O$ (Htrz = 1,2,4-4*H*-triazole; trz = 1,2,4-triazolato). *Chem. Mater.*, **1994**, *6*, 1404–1412.

[29] Le Bail, A.; Whole powder pattern decomposition methods and applications: A retrospection. *Powder Diffr.* **2005**, *20***,** 316–326.

[30] Haasnoot, J. G.; Vos, G.; Groeneveld, W. L.; 1,2,4-triazole complexes III: complexes of transition metal(II) itrates and fluoroborates, *Z. Naturforsch B,* **1977**, *32*, 1421–1430.

[31] Grosjean, A.; Négrier, P.; Bordet, P.; Etrillard, C.; Mondieg, D.; Pechev, S.; Lebraud, E.; Létard, J.-F.; Guionneau, P.; Crystal structures and spin crossover in the polymeric material $[Fe(Htrz)_2trz](BF_4)$ including coherent-domain size reduction effects. *Eur. J. Inorg. Chem.* **2013**, 796-802.

[32] Suslick, K. S.; Price, G. J.; Applications of ultrasounds to materials chemistry. *Annu. Rev. Mater. Sci.* **1999**, *29*, 295−326.

[33] Vancleef, A.; Seurs, S.; Jordens, J.; Van Gerven, T.; Thomassen, L. C. J.; Braeken, L.; Reducing the Induction Time Using Ultrasounds and High-Shear Mixing in a Continuous Crystallization Process. *Crystals* **2018**, *8*, 326.

[34] Evrard, Q.; Houard, F.; Daiguebonne, C.; Calvez, G.; Suffren, Y.; Guillou, O.; Mannini, M.; Bernot, K.; Sonocrystallization as an Efficient Way to Control the Size, Morphology, and Purity of Coordination Compound Microcrystallites: Application to a Single-Chain Magnet. *Inorg. Chem.* **2020**, *59*, 9215-9226

[35] Jordens, J.; Appermont, T.; Gielen, B.; Van Gerven, T.; Braeken, L.; Sonofragmentation: Effect of Ultrasounds Frequency and Power on Particle Breakage. *Cryst. Growth Des*. **2016**, *16*, 6167−6177.

[36] Suslick, K. S.; Hammerton, D. A.; Cline, R. E.; Sonochemical hot spot. *J. Am. Chem. Soc.* **1986**, *108*, 5641−5642.

[37] Luque de Castro, M. D.; Priego-Capote, F.; Ultrasounds-assisted crystallization (sonocrystallization). *Ultrason. Sonochem*. **2007**, *14*, 717−724.

[38] Kim, H. N.; Suslick, K. S.; The Effects of Ultrasounds on Crystals: Sonocrystallization and Sonofragmentation. *Crystals* **2018**, *8*, 280.

[39] Jordens, J.; Bamps, B.; Gielen, B.; Braeken, L.; Van Gerven, T.; The effects of ultrasounds on micromixing. *Ultrason. Sonochem*. **2016**, *32*, 68−78.

For table of contents use only:

Title: Optimized local synthetic conditions induce size reduction and phase purification in $\{[Fe(Htrz)_2(trz)](BF_4)\}_n$ spin crossover particles

Authors: Tristan CASTEL, Anaïs MARCHETTI, Félix HOUARD, Nathalie DARO, Mathieu MARCHIVIE, Guillaume CHASTANET, Kevin BERNOT.

Synopsis: This paper explores new template-free syntheses of spin crossover nanoparticles by controlling the local reaction conditions using a one-pot approach (high local concentration), and pulsed ultrasound waves (high local temperature).